Chapter 5

Enhanced hydrogen evolution reaction on polypyrrole/Ni-doped NASICON PPy/NFS(Ni) composites modified electrodes.

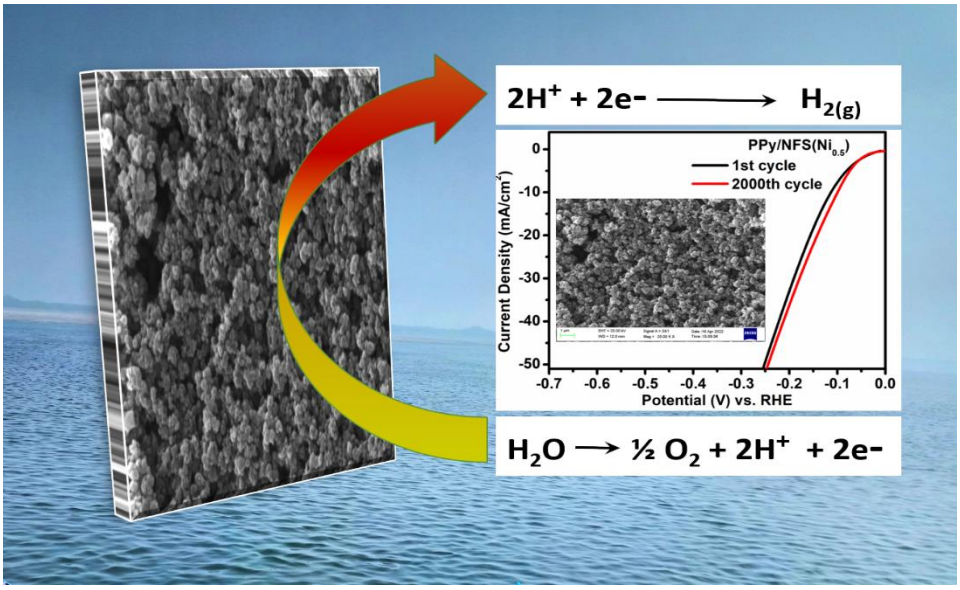

This chapter further explores the enhanced catalytic activity towards HER of PPy/Ni-doped NFS composites via incorporating various percentages of Ni doping into the NFS. The obtained results significantly highlight the role of Ni doping in NFS for enhancing the active sites and ease of charge transfer resulting in excellent HER activity by PPy/NFS(Ni) composites. The improved HER catalytic activity of PPy/NFS(Ni) composites is comparable to the noble metal Pt. It can be used as an alternative to the costly noble metal Pt catalyst for HER.

5.1 Introduction

For the past few centuries, fossil fuels have been used as a primary energy source despite having many disadvantages- limited resources, environmental pollution, global warming, and a lack of traditional fossil fuels in the foreseeable future.[149] The rate of fossil fuel use will soar because of the projected increase in world energy demand to around 27 TW in 2040, resulting in a more significant accumulation of CO_2 in the atmosphere.[149], [150] Even though fossil fuels are fulfilling the energy need in the following decades, their finite reserves and the adverse effects on the global climate prevent them from achieving the world's sustainable development objectives.[150] To resolve the current environmental pollution challenges while solving the energy deficit difficulties, we must implement an alternative energy system that is clean and renewable[149], [150]. In this regard, developing sustainable and clean energy systems has been a matter of extreme urgency. In the past few decades, various countries worldwide have devoted significant efforts toward producing carbon-free renewable energy resources (including hydraulic power, solar, and wind) that have been investigated as sustainable and clean alternatives to conventional fossil fuels.[150], [151] Apart from the advantages of being environmentally friendly, their application is limited by temporal and spatial intermittencies due to time and weather-dependent nature, expensive maintenance, and low energy efficiency.[151] As a result, applying other practical solutions to deal with these issues is crucial. With the unique advantages of the highest volumetric and gravimetric energy density, hydrogen (H_2) is a viable choice for sustainable and next-generation green and carbon-free clean energy carriers that could change the future global energy structure requirement.[149], [60], [190] This fuel has the potential to swap out conventional fuels and store them as additional energy with the help of a system that connects to the renewable energy system for energy demands. [190] Several resources, including biomass, petroleum, natural gas, coal, and

water, can produce H_2.[151] Despite being a renewable resource, biomass cannot deliver significant energy demands.[150], [151] Highly efficient and ecologically acceptable techniques must be used to manufacture clean and economically feasible hydrogens. The two most promising methods in this regard are electrochemical water splitting [153] and photoelectrochemical [152], which rely on unlimited water supplies and can produce large amounts of high-purity H_2. Electrochemical water splitting is more appealing because it is more flexible and productive than photoelectrochemical water splitting.[150], [153]

Conventionally, Pt (noble metal) and Pt-based catalysts show high efficiency towards electrochemical hydrogen evolution reaction (HER), but steep costs and lack of reserves constrain their widespread use.[154] In addition to examining other options like earth-abundant catalysts having the merits of high efficiency and cost-effectiveness, numerous research organizations worldwide are making significant efforts to increase the consumption efficiency of the noble-metal-based catalyst.[60], [150] Various materials, including noble metals and their combination, [191] metals [155] bimetallic [155] metal oxide [149] sulfides,[60] phosphides [155], [156], tellurides [157], nitride [155], [187], carbides [155], [192], metal alloy [155] carbon-based materials like CNTs [159] and GOs [158], metal-organic framework [193] have been reported so far as efficient catalysts for electrochemical HER. However, the exorbitant prices of noble metals, inactivity of metals and metal-based electrocatalysts, electrode poisoning after some time, and metal corrosion in harsh situations, i.e., acidic and basic conditions and their inefficiency at the industrial level (due to low hydrogen economy) limit their uses [160]. One of the effective approaches to overcome the issues mentioned above is using composite materials, which are cost-effective, noble (Pt is used as the benchmark for HER electrocatalyst with very high activity) and toxic metal-free, environmentally friendly, and highly stable. [60], [149], [150], [151] The merits of electrochemical HER for clean and

sustainable hydrogen (H_2) production include feasibility for a large-scale application, high purity H_2, unrestricted water resources, and high stable output.[150], [151], [190] Due to the vibrant superiority of morphological and compositional as well as structural flexibilities and modification diversity, conducting polymer composite materials have been recognized as potential candidates for catalyzing HER in recent years [161], [162], [164]. Also, conducting polymers have advantages over others concerning cost-effectiveness, processibility, non-toxic, and environmentally friendly. [161], [162], [164], [165] Conducting polymers, specially polyaniline [165], [194], polyindole [167], polythiophene [166], poly-o-aminophenol [167], poly(3,4-ethylenedioxythiophene) (PEDOT) [168] and polypyrrole [164], [167] along with their composites have been explored for HER. Previous reports evidenced that polypyrrole (PPy) is a potential candidate for electrocatalytic energy conversion. [169], [170] The electron-rich nitrogen of PPy has a high affinity toward metals. [164], [167], [169] Ni-doped NASICON structure $Na_3Ni_xFe_{(2-x)}(PO_4)(SO_4)_2$, on the other hand, has a very high affinity for water. Moreover, the conjugation in multiple bonds of heterocyclic moieties in PPy enhances the capability of sharing electrons of the electron-rich nitrogen center with the electron-deficient center of NFPS(Ni_x), making it a good candidate for easy charge transfer. Additionally, the positive charge centers on the polymer backbone easily interact with the electron-rich centers. [167] These unique features make the composite material, PPy/NFPS(Ni_x), best suitable for electrochemical HER application.

In the current work, PPy/NFPS-Ni composite was synthesized via in-situ chemical oxidative polymerization by incorporating NFPS(Ni_x) into the polypyrrole at the monomeric level. The doping of Ni is made in pure NFPS. Polymerization is done by taking a fixed amount of pyrrole (Py) monomer with oxidizing agent APS (ammonium persulphate). As-synthesized composites with different amounts of $Na_3Ni_xFe_{(2-x)}(PO_4)(SO_4)_2$ (NFPS(Ni_x); x = 0.1, 0.2, 0.5, 0.8, 1.0) are

symbolized as PPy/NFPS($Ni_{0.1}$), PPy/NFPS($Ni_{0.2}$), PPy/NFPS($Ni_{0.5}$), PPy/NFPS($Ni_{0.8}$), and PPy/NFPS($Ni_{1.0}$). The structural and compositional characterizations were done with the help of XRD, FT-IR, XPS, and TGA. SEM was used for morphological illustrations. The as-synthesized composites were then examined for electrochemical HER in 0.5 M H_2SO_4 electrolytic solution with modified Torrey paper as the working electrode. Additionally, using BET, the specific surface area of the PPy/NFPS($Ni_{0.5}$) (optimized HER catalyst), pristine PPy, and NFPS($Ni_{0.5}$) have been examined. PPy/NFPS($Ni_{0.5}$) exhibited excellent HER activity with a remarkably lower onset potential of -13 mV vs. RHE and a lower Tafel slope (58 mV dec^{-1}). The catalyst also offers a current density of 10 mA/cm^2 at a considerably low overpotential (-111 mV) vs. RHE and excellent long-lasting environmental stability and catalytic activity.

5.2 Experimental section

Materials: Pyrrole monomer (Sigma Aldrich), ammonium persulphate (Merck, ≥ 98%), Mohr's salt (Sigma Aldrich, ≥ 99%), sodium hydrogen phosphate (Merck, ≥ 99%), sodium carbonate (Sigma Aldrich, ≥ 99.5%), Nickel sulfate (Merck, ≥ 98%).

Synthesis methods:

Synthesis of NFPS and NFPS(Ni_x)

The NFPS was synthesized by the chemical co-precipitation method. [171] Now, the synthesis of Ni-doped NFPS (NFPS($Ni_{0.5}$)) was carried out by a simple chemical co-precipitation method: First, 1.5 M of $(NH_4)_2Fe(SO_4)_2 \cdot 6H_2O$ aqueous solution was prepared in 100 mL, followed by stirring a 90 ºC for 1 hour. Then, 1 M Na_2HPO_4 was supplied to the above solution with further 2 hours of stirring. Afterward, 0.5 M nickel sulfate was added, followed by 2 M sodium carbonate to the above reaction mixture, resulting spontaneous evolution of CO_2. The solution

mixture pH was balanced by ammonia addition, where precipitation occurred. The as-obtained dried yellow residue was calcined at 500 ºC for 12 hours to get crystalline NFPS($Ni_{0.5}$).

The other Ni-doped NFPS ratios were synthesized similarly by varying nickel sulfate amounts.

Synthesis of composites of polypyrrole with the incorporation of NFPS(Ni_x)

The PPy/NFPS(Ni_x) composites were synthesized using the In-Situ chemical oxidation method. A predetermined amount of Py monomer (0.5 ml) was first mixed with 70 ml of ice-cold DI water while continuously stirring. Next, the previously synthesized nano NFPS(Ni_x) (25 mg, 5% weight ratio of Py: NFPS(Ni_x)) was supplied to the above solution. The reaction mixture was stirred for 2 hours to confirm adequate dispersal and interaction of Py monomer and NFPS(Ni_x). Next, 30 mL of 100 mM APS solution was supplied slowly and dropwise to the reaction mixture for polymerization under stirring conditions. The stirring of the reaction mixture continued for another 2 hours after adding APS. It was then left overnight as such for the completion of polymerization. The subsequent day, the formed composite was given repeated washing and filtering with DI water and ethanol to remove any residual impurities and unreacted monomers. The materials were then dried at 50 ºC in the oven for 24 hours before using as active electrode materials.

The synthesis of other compositions of PPy/NFPS(Ni_x) composites was done using a similar reaction condition by taking variable amounts of Ni in NFPS.

Electrode fabrication:

Initially, 4 mg per mL of composite materials was dispersed in the ethanol-water mixture (2:3 V/V) to make the slurry ink. The ink was exfoliated for better dispersion of materials using ultra-sonicated for 2 hours. It was then cast on unit-area Torrey paper, and the modified

electrode was dried at 60 °C for 24 hours under proper vacuum. The electrode was then used in HER applications as an active working electrode.

5.3 Results and discussions:

Structural characterizations:

The crystal structure and phase analysis of as-synthesized materials is done through the X-ray diffraction technique. As shown in figure 5.1 (a), pure NFPS exhibits a rhombohedral phase [171] with space group '$R\bar{3}c$', varying the Ni doping concentration in pure NFPS did not cause any phase change except for some lattice defects. The acceptable percentage of ionic radii difference (D_r) [195] is around 30%, where, $D_r = \frac{R_s - R_d}{R_s}$, and R_s, R_d defines the ionic radius of substituted and doped ions, respectively. In our case, D_r~11.5%, and thus we can conclude that Ni^{2+} ions can easily replace Fe^{2+} ions in the NFPS host matrix without any significant effect on the parent crystal structure. However, when a relatively smaller ion (Ni^{2+}) replaces a larger ion (Fe^{2+}), the effective crystal volume is expected to shrink, which is evident in the redshift of higher angle diffraction peaks, as shown in figure 5.1 (a) inset. The average crystallite size of NFPS and Ni-doped NFPS matrices has been estimated using the Debye-Scherrer formula, [195] $D = \frac{0.89\lambda}{\beta Cos\theta}$ where λ denotes the X-ray wavelength (1.54 Å) used, and β is the integrated peak width at half maxima. It has been found that NFPS($Ni_{0.5}$) has the highest average crystallite size~50.26 nm, among all the samples. In figure 5.1 (b), a broad peak of PPy shows amorphous nature in an XRD pattern that is matched with the earlier reports. [174] In composites, some diffraction peaks over the PPy amorphous background can be seen, and these peaks correspond to crystalline NFPS($Ni_{0.5}$) having a high scattering factor. Thus, XRD patterns evidenced the successful synthesis of PPy, NFPS, Ni-doped NFPS, and their composites.

Table 5.1: Structural information of synthesized samples

Sample	**NFPS**	**NFPS($Ni_{0.1}$)**	**NFPS($Ni_{0.2}$)**	**NFPS($Ni_{0.5}$)**	**NFPS($Ni_{0.8}$)**	**NFPS($Ni_{1.0}$)**
Crystal Phase	Rhombohedral					
Space group	$R\bar{3}c$					
Avg. crystallite size (nm)	48.9	49.1	47.6	50.3	39.1	35.2

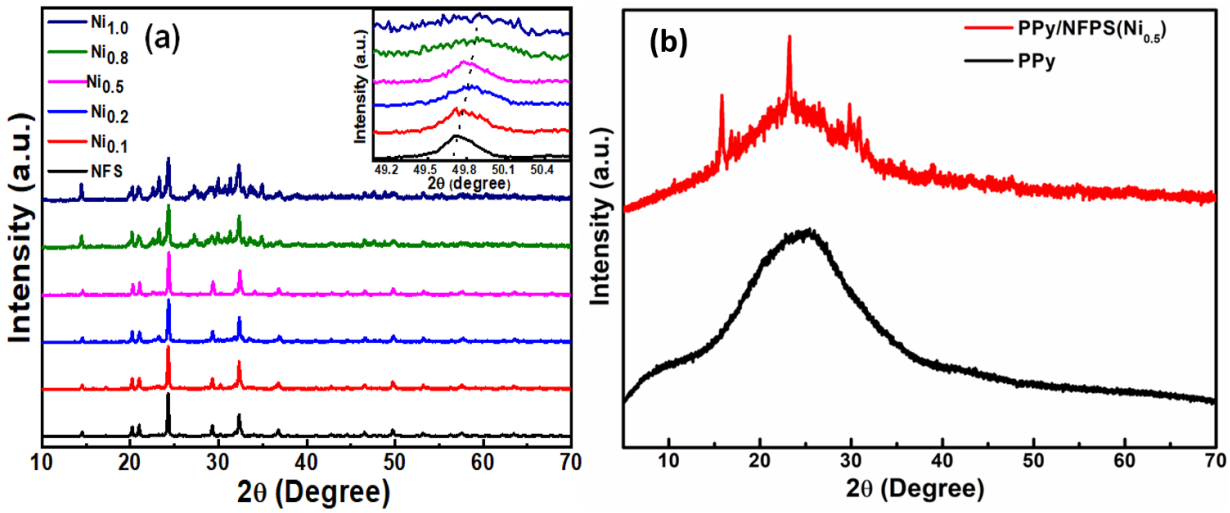

Figure 5.1: (a) XRD patterns corresponding to pure NFPS and Ni-doped NFPS with different concentrations, (b) XRD of pure PPy, and composite PPy/NFPS($Ni_{0.5}$).

Different functional groups, moieties, and molecular structures are investigated with the help of FT-IR in transmittance mode using KBr, as depicted in figure 5.2(a). Table 5.2 contains the primary and characteristic peaks of pure PPy and NFPS, which provides evidence that PPy and NFPS are formed. In the case of composite materials, all the primary and characteristic peaks of individual components are there, along with some peak shifting due to interaction between PPy and Ni-doped NFPS. It might also result from the variations in the environment of different

functional groups and moieties. Additionally, different Ni doping levels in NFPS in PPy/NFPS(Ni_x) composites cause causes variations in peak intensities.

Table 5.2: Different functional groups in PPy and NFPS as analyzed from FT-IR spectra

Peaks (cm^{-1})	**PPy Functional Groups**	**References**
618	Vibration in out-of-plane of N-N	[172]
783	ring bending in PPy	[172]
934	C-H out of the plane deformation	[172]
1045	C-H in-plane bending (PPy-ring)	[172]
1179	Py ring (breathing) vibration	[172]
1384	PPy ring vibrations	[172]
1457	stretching vibration of C-N in the Py ring	[172]
3423	C-C stretching in the pyrrole ring	[172], [173]
Peaks (cm^{-1})	**NFPS Functional Groups**	
500-750	PO_4^{3-}/ SO_4^{2-} bending modes of vibration	[171]
989	PO_4^{3-} symmetric/asymmetric stretching vibration	[171]
1047	SO_4^{2-} symmetric stretching vibration	[171]
1139	SO_4^{2-} asymmetric stretching vibration	[171]
3443	-OH stretching vibration	[171]

After structural characterization, thermal stability quantification for NFPS($Ni_{0.5}$) of different components having dissimilar flame retardancy is investigated with the help of TGA. Figure 5.2(b) shows the TGA curve of pristine PPy, NFPS($Ni_{0.5}$), and PPy/NFPS($Ni_{0.5}$) (optimized ratio for HER) as a function of temperature. The curve also gives a clear-cut idea of weight loss

at various stages to categorize the degradation processes. Initially, 8% weight loss at a temperature ranging from 50-110 ºC is due to the loss of water present in the materials. The saturation in weight appears up to 200 ºC. After that, polymer nanocomposite materials' degradation starts and degrades up to 450 ºC with a weight loss of about 36%. The weight loss of composite materials in the temperature range of 450 ºC to 730 ºC can be accredited to the combustion leaving behind a residue of about 5% in PPy/NFPS($Ni_{0.5}$). Almost similar trends are also observed in the case of pure PPy [174], having a residual of about 2% ash after 730 ºC. However, the Ni-doped NFPS is fairly thermally stable up to 730 ºC, as depicted in the TGA plot in figure 5.2(b). So, it is perceivable from the TGA curve that PPy/NFPS($Ni_{0.5}$) has better stability to temperature than pristine PPy because of the incorporation of NFPS($Ni_{0.5}$) in the polymer matrix.

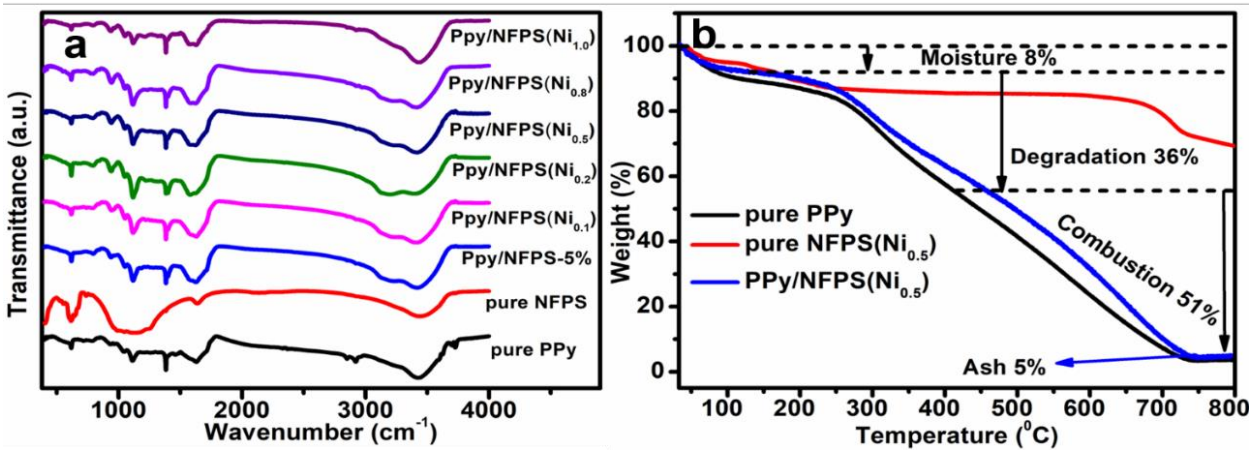

Figure 5.2: (a) FTIR spectra of pristine PPy, pristine NFPS and its composites with varying doped amounts of Ni in NFPS, (b) Thermogravimetric Analysis (TGA) curve of pristine PPy, pristine NFPS($Ni_{0.5}$), and PPy/NFPS($Ni_{0.5}$) composite.

The chemical composition and the oxidation state of each element of catalytic material PPy/NFPS($Ni_{0.5}$) were investigated using XPS. The XPS survey spectrum of PPy/NFPS($Ni_{0.5}$) confirms the existence of each elements C, O, N, Fe, S, Ni, Na, and P, as displayed in figure

5.3(a). The C1s spectra (figure 5.3(b)) show four deconvoluted peaks, where three are located at binding energy 283.8 eV, 285.1 eV, and 288.0 eV associated with C=C, C-N, and C-C of the PPy unit, and one at 286.1 eV related to C-O corresponding to oxidative polymerization.[175] The XPS peaks of N1s [175] (figure 5.3(c)) are deconvoluted into three groups which are imine (-N=), pyrrolic (-NH-), and charged nitrogen for three respective binding energies at 399.5 eV, 400.0 eV, and 401.9 eV. The high-resolution O1s (figure 5.3(d)) deconvoluted for $(PO_4)^{3-}$ at binding energy 530.5 eV, P=O and/or S=O at 531.4 eV, $(SO_4)^{2-}$ at 532.6 eV and -OH at 533.6 eV corresponding to NFPS($Ni_{0.5}$) be due to oxidative polymerization and adsorbed water. The high-resolution XPS peaks of Fe2p split into two-part Fe $2p_{3/2}$ and Fe $2p_{1/2}$ and deconvoluted, which exhibits two binding energy values at 711.1 eV and 725.2 eV, which corresponds to Fe^{2+} and 713.4 eV and 728.9 eV for Fe^{3+} indicating +2 and +3 oxidation state of Fe in PPy/NFPS($Ni_{0.5}$) [176], [177]. The typical high-resolution peaks of Ni 2p (figure 5.3(g)) split into Ni2p1/2 and Ni2p3/2 and their corresponding fitted profile indicating both Ni^{2+} and Ni^{3+}. [196] The +3 oxidation state of both Fe and Ni might be because of oxidative polymerization and, hence, some interaction between PPy and NFPS($Ni_{0.5}$) in composite PPy/NFPS($Ni_{0.5}$). [196] The fitted XPS peaks of S 2p have two parts S 2p1/2 and S 2p3/2, located at 168.0 eV and 168.9 eV, respectively, conforming to $(SO_4)^{2-}$ environments.[177] Likewise, P 2p XPS peaks deconvoluted into two peaks for P 2p1/2 (133.4 eV) and P 2p3/2 (134.3 eV), respectively, which is attributed to $(PO_4)^{3-}$ environments of NFPS($Ni_{0.5}$) part of the composite.[176] The above XPS fitting confirms the elemental chemical state present in the PPy/NFPS($Ni_{0.5}$) composite.

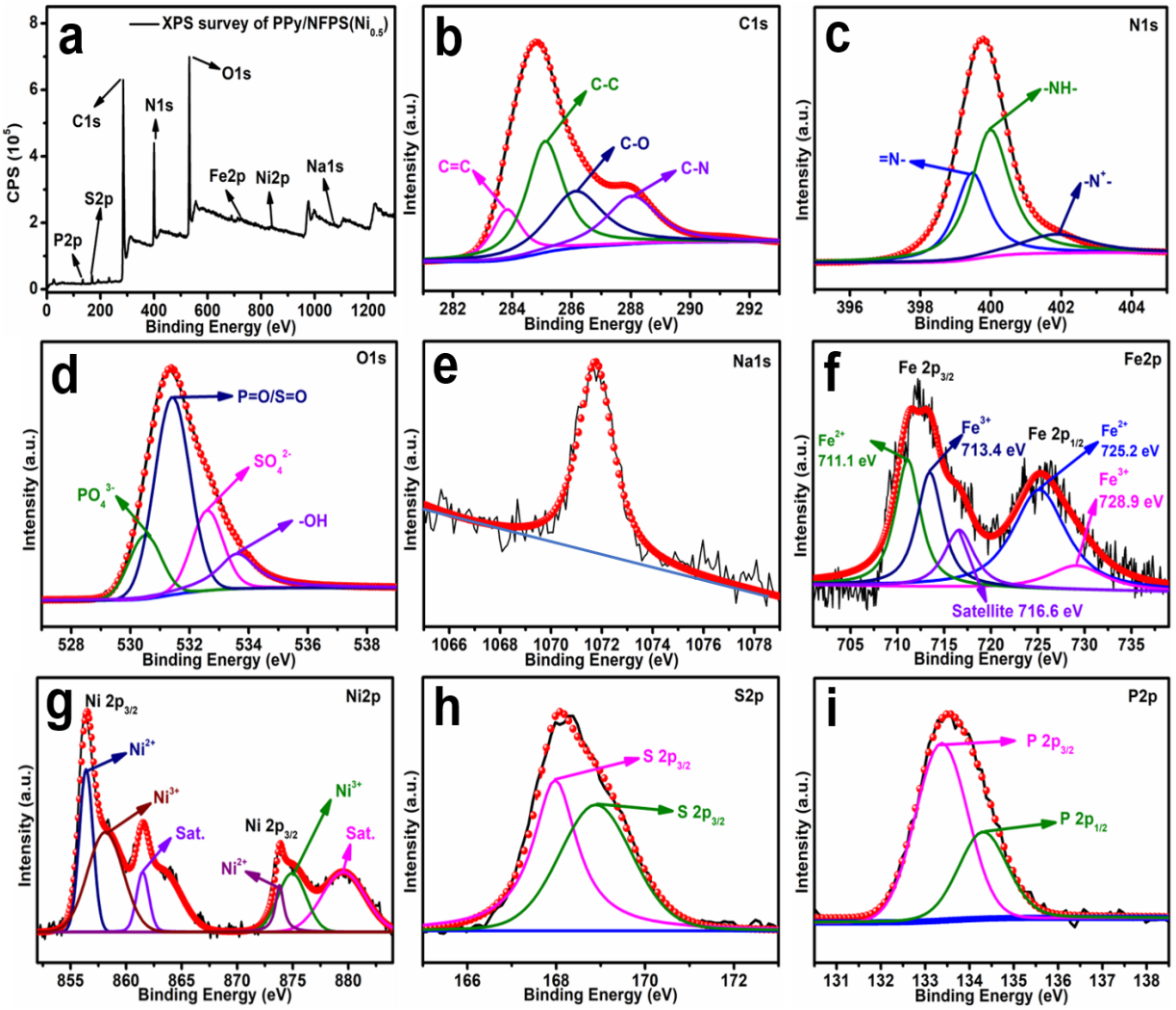

Figure 5.3: XPS spectra of PPy/NFPS($Ni_{0.5}$) composite (a) XPS survey of PPy/NFPS($Ni_{0.5}$) composite, deconvoluted high-resolution XPS of (b) C1s, (c) N1s, (d) O1s, (e) Na1s, (f) Fe2p, (g) Ni2p, (h) S2p and (i) P2p.

Surface Area Analysis:

The catalyst properties, such as electron transfer abilities and mass transfer, excessively depend on materials' surface area and porosity. Hence to get more insight into the electrocatalytic materials, adsorption isotherm and BET was measured for surface area analysis with the help of N_2 (at 77 K) adsorption-desorption isotherm (figure 5.4). A notable increase in the BET surface area signals the accessibility of more active sites that should boost catalytic proficiency.[178] The mesoporous nature of the catalytic materials is shown by the isotherm of type IV having a hysteresis loop. [187] The overlapping of adsorption-desorption isotherm causes the process to be reversible at the relative pressure ($P/P_0 < 0.65$) for all three catalysts. An important hysteresis loop with no adsorption-desorption overlapping in the upper range (0.65-1.0 *P/P0*) might also account for the mesoporous structure of PPy/NFPS($Ni_{0.5}$). According to the BET plot, the specific surface areas for pristine PPy (figure 5.4(a)), pristine NFPS($Ni_{0.5}$) (figure 5.4(b)), and PPy/NFPS($Ni_{0.5}$) (figure 5.4(c)) are 53.9 $m^2\ g^{-1}$, 17.8 $m^2\ g^{-1}$, and 290.4 $m^2\ g^{-1}$, respectively. These findings demonstrate that PPy/NFPS($Ni_{0.5}$) has a surface area more than five times that of pure PPy. It means that NFPS($Ni_{0.5}$) makes the PPy matrix more porous and exfoliates, increasing the surface area of composites (figure 5.4(c)). Using the Brunauer-Joyner-Halenda (BJH) theory, the PPy/NFPS($Ni_{0.5}$) pore size distribution has been examined (figure 5.4(d)), with majorities of pore size lying in the 15-60 nm range (mean pore size 36.8 nm), indicating the mesoporous property of the catalytic materials. When NFPS($Ni_{0.5}$) is incorporated, the pore capacity of PPy increases from 1.24 $cm^3\ g^{-1}$ in pure PPy to 8.97 $cm^3\ g^{-1}$ in PPy/NFPS($Ni_{0.5}$), showing that PPy has become more exfoliated in the composite. Therefore, incorporating NFPS($Ni_{0.5}$) into the PPy causes excessive porosity. This increased porosity generates additional active sites for interacting with the ions, which facilitates and speeds up electron transport for catalytic activity.

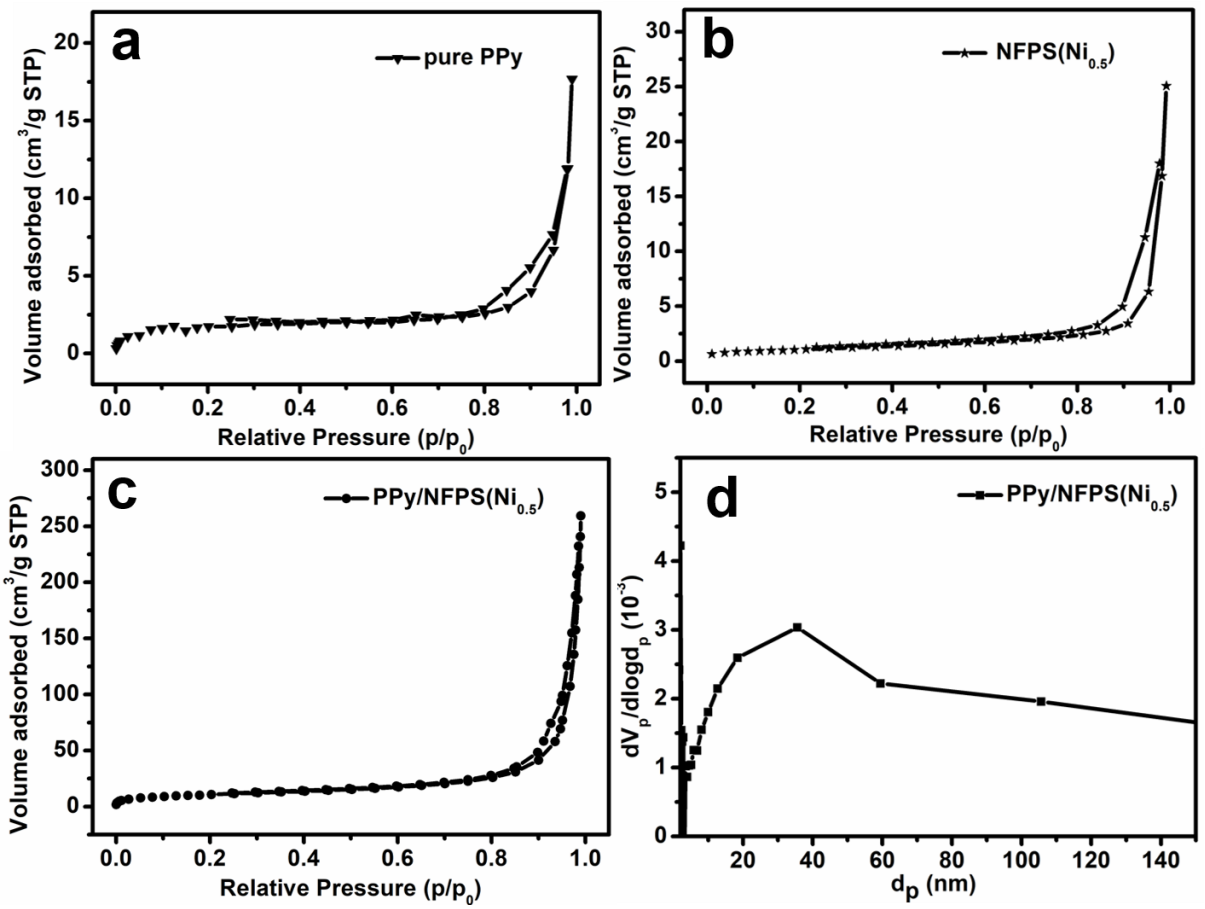

Figure 5.4: N_2 isotherm of (a) pristine PPy, (b) pristine NFPS($Ni_{0.5}$) and (c) PPy/NFPS($Ni_{0.5}$), (d) curve of pore-size distribution of PPy/NFPS($Ni_{0.5}$).

Morphological Characterization:

SEM is utilized for the catalytic materials' morphological and compositional characterization. The SEM images of pristine PPy, pristine NFPS, and PPy/NFPS-5% (optimized ratio for NFPS) are depicted in Figure 5.5(a, b, and c), respectively. Pure PPy displays a sphere-like morphology with about 300 nm average diameter, whereas pristine NFPS displays a granular morphology of irregular shapes and sizes. The PPy/NFPS-5% also shows a spherical morphology with a smaller diameter than PPy (figure 5.5(c)). The SEM image of NFPS($Ni_{0.5}$) in figure 5.5(d) shows flakes and granules-like morphology having irregular sizes and shapes. The

PPy/NFPS($Ni_{0.5}$) in figure 5.5(e) shows the uniform morphology and spherical shape. Also, the average diameter of PPy/NFPS($Ni_{0.5}$) (~150 nm) is reduced than pure PPy and PPy/NFPS-5%, implying more availability of active catalytic sites. As seen from the PPy/NFPS($Ni_{0.5}$), PPy is more diffused with NFPS($Ni_{0.5}$) and with each other, indicating interactions to some extent which can also be seen from the diffraction pattern of XRD of composite. The mapping (figure 5.5(f)) and EDAX (figure 5.5(g)) confirm the presence of different elements and their uniform distribution throughout the composite materials PPy/NFPS($Ni_{0.5}$). The inset of figure 5.5(f) shows an approximate percentage of the elements present in the PPy/NFPS($Ni_{0.5}$).

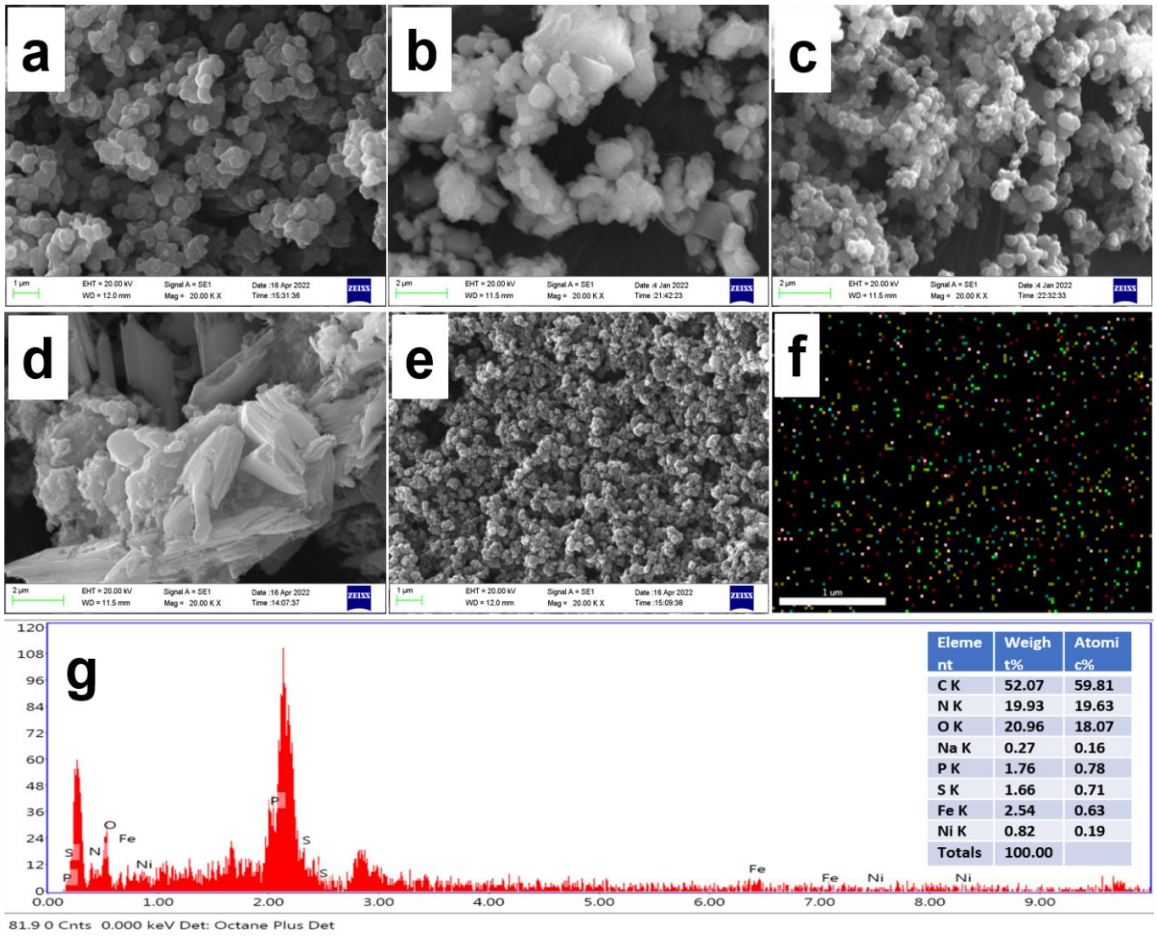

Figure 5.5: SEM image of (a) pristine PPy, (b) pristine NFPS, (c) PPy/NFPS-5% (optimized ratio for NFPS), (d) NFPS($Ni_{0.5}$), (e) PPy/NFPS($Ni_{0.5}$), (f) elemental mapping of PPy/NFPS($Ni_{0.5}$), (g) EDAX of PPy/NFPS($Ni_{0.5}$).

Electrochemical Characterization:

Thanks to extended π-conjugation, the environmentally stable and ecologically friendly PPy shows excellent electrical properties among conducting polymers, although it exhibits weak HER activity. In comparison to pure PPy, the catalytic activity toward HER is multiplied in the case of composites. The HER catalytic activity of various PPy/NFPS(Ni_x) composite ratios was examined with the help of electrochemical techniques using the LSV polarization curve and Tafel slope, as depicted in figure 5.6. The LSV of all the composite materials, pristine PPy, pristine NFPS, and 20% Pt/C were done at a cathodic scan rate of 10 mV/s. The Relative hydrogen evolution for various PPy/NFPS(Ni_x) composite electrode materials, including pure NFPS, pure PPy, blank Torrey, and 20% Pt/C is shown using the LSV polarization curve in figure 5.6(a). The onset overpotential of various electrode materials is -248 mV for pure PPy, -79 mV for pure NFPS, -46 mV for PPy/NFPS($Ni_{0.1}$), -101 mV for PPy/NFPS($Ni_{0.2}$), -13 mV for PPy/NFPS($Ni_{0.5}$), -21 mV for PPy/NFPS($Ni_{0.8}$) and -42 mV for PPy/NFPS($Ni_{1.0}$). The amount of Ni in the NFPS was optimized to analyze the onset potential fluctuation in HER and obtain the superior J (current density) value for PPy/NFPS($Ni_{0.5}$) composite. Among all the electrode materials, PPy/NFPS($Ni_{0.5}$) shows the best HER performance (figure 5.6(a)). The catalytic materials PPy/NFPS($Ni_{0.5}$) offers the lowest onset potential of -13 mV vs. RHE compared to pristine PPy and other composite ratios. Additionally, it exhibits a current density of 10 mA/cm^2 at a lower overpotential (η) of -111 mV vs. RHE compared to other electrode materials. The conjugation in multiple bonds of heterocyclic moieties in PPy enhances the capability of sharing electrons of the electron-rich nitrogen center with the electron-deficient center of NFPS(Ni_x), making it a good candidate for easy charge transfer. Ni-doping in NFPS can cause nearby active sites to have insufficient electrons, stimulating hydrogen adsorption and raising surface hydrogen coverage [197]. Due to this reason, there is a tremendous increase

in effective catalytic active sites and a greater probability of HER. Additionally, the positive charge centers on the polymer backbone can easily interact with the electron-rich centers. [167] These might be the solid reason for synergism between PPy and NFPS(Ni_x) for easy charge transfer through the composite materials PPy/NFPS(Ni_x), resulting in excellent HER catalytic activity. In comparison to the PPy/NFPS($Ni_{0.5}$), the other ratios of the PPy/NFPS(Ni_x) composites exhibit poorer catalytic activity, which can be seen in figure 5.6(a).

Table 5.3: Performance comparison of recently published electrocatalyst based on conjugated polymer for HER

S.No.	Electrocatalyst	Electrolyte medium	Onset potential (mV) vs. RHE	η at 10 mA/cm^2	References
1	PPy/$ZnWO_4$	0.5 M H_2SO_4	---	-543 mV	[42]
2	PPy+MoS_2 Mix	0.5 M $HClO_4$	-0.4 V (SCE)	---	[181]
3	SiO_2/PPyNTs–CFs	1.0 M NaH_2PO_4/Na_2HPO_4	-70 mV	~ -183 mV	[180]
4	Co_3O_4/Ppy/MWCNT	0.1 M KOH	-287 mV	-490 mV	[183]
5	PPy@SiO_2-HMS	1.00 M KOH	-61 mV	-123 mV	[164]
6	(Ppy/MoS_2)16-CC	0.5M H_2SO_4	-194 mV	-280 mV	[162]
7	PtNPs@MXene/PPy	0.5M H_2SO_4	---	-40 mV	[184]
8	PANI-Nbs	1 M KOH	-51 mV	-202 mV	[185]
9	poly[K_x(Ni-ett)]	0.5 M H_2SO_4	-250 mV	-360 mV	[198]
10	PANI/$MnMoO_4$ -10	1.0 M KOH	---	-155 mV	[199]
11	PPy/NFPS-5%	0.5 M H_2SO_4	-26 mV	-206 mV	Chapter 4
12	PPy/NFPS($Ni_{0.5}$)	0.5 M H_2SO_4	-13 mV	-111 mV	This work

Although HER catalytic activity for PPy polymer-based materials still performs less significantly than Pt-based catalysts, the HER performance of PPy/NFPS($Ni_{0.5}$) displays better and more effective electrochemical activity, which can be comparable with Pt-based catalysts. Additionally, it outperforms most of the recently published articles related to the subject for the HER, tabulated in Table 5.3. High bandgap energy is indicated by a high Tafel slope, which yields a high overpotential since high energy is mandatory to induce activity and vice versa. The Tafel slope of each catalytic material was obtained using the LSV curve. The computation relies on fitting into the Tafel equation (i.e., $\eta = a + b \log (J)$, where '*J*' denotes the current density and 'b' represents the Tafel slope), where a lower Tafel slope indicates greater HER activity and a slight increase in overpotential. [200], [201], [202] From figure 5.6(b), the PPy/NFPS($Ni_{0.5}$) shows the smallest Tafel slope value of 58 mV dec^{-1} in comparison to the other ratios of PPy/NFPS(Ni_x) composites, while 20% Pt/C offers a Tafel slope value of 34 mV dec^{-1}. Tafel slope value of other PPy/NFPS(Ni_x) composite ratios reveals 154, 108, 121, and 168 mV dec^{-1}, respectively, for PPy/NFPS($Ni_{0.1}$), PPy/NFPS($Ni_{0.2}$), PPy/NFPS($Ni_{0.8}$), and PPy/NFPS($Ni_{1.0}$) as displays in figure 5.6(b). The LSV curve of pristine PPy, pristine NFPS, PPy/NFPS-5%, and PPy/NFPS($Ni_{0.5}$) with 20% Pt/C are presented for comparison purposes in figure 5.6(c), and their Tafel plots are shown in figure 5.6(d). PPy/NFPS($Ni_{0.5}$) has a lower onset overpotential and Tafel slope value than other ratios, making it a better electrode material for HER with high activity. The Butler-Volmer equation calculates the Tafel slope for three limiting HER reactions. The multistep HER process at the cathode is susceptible to changes in electrolyte pH. The HER mechanism in the acidic medium can be described via different pathways as follows:[186], [207]

$H_3O^+ + e^- + A \rightarrow HA + H_2O$ (Volmer reaction; 120 mV dec^{-1}) (eq. 5.1)

$HA + H_3O^+ + e^- \rightarrow H_2 + H_2O + A$ (Heyrovsky reaction; 38 mV dec^{-1}) (eq. 5.2)

$HA + HA \rightarrow H_2 + 2A$ (Tafel reaction; 29 mV dec^{-1}) (eq. 5.3)

A stands for the catalyst's active site, and HA indicates adsorbed hydrogen atoms on the active sites. The HER follows either Volmer-Heyrovsky or Volmer-Tafel pathway in any medium. A Tafel slope value of 58 mV dec^{-1} signifies that the PPy/NFPS($Ni_{0.5}$) follows the Volmer-Heyrovsky-subjugated paths during the HER process from the catalytic surface. Whatever the route it follows, the reaction passes through the hydrogen adsorption on the catalysts' surface. [203] As a result, the critical parameter for HER kinetics is the hydrogen adsorption Gibbs free energy (ΔG_{Had}). [188] Pt has the free energy for adsorbed hydrogen close to zero, which causes the best catalytic activity for HER. If the ΔG_{Had} value is too negative, it can limit the evolution of hydrogen molecules by limiting the Tafel or Heyrovsky steps. On the other hand, if the ΔG_{Had} value is too positive, the Volmer step is slowed down as intermediate hydrogen formation becomes challenging. An ideal HER catalyst should therefore have an optimal ($\Delta G_{Had} \sim 0$) hydrogen intermediate bonding energy that binds hydrogen atoms neither too weakly nor too strongly. [188], [204] The presence of Ni-doping in NFPS promotes the value of ΔG_{Had} close to zero resulting in fast adsorption-desorption of hydrogen on active sites of the catalyst. Therefore, doped NFPS with Ni enhances the HER activity. Hence, it shows how the NFPS($Ni_{0.5}$) embedded composite has increased catalytic behavior and synergistic performance.

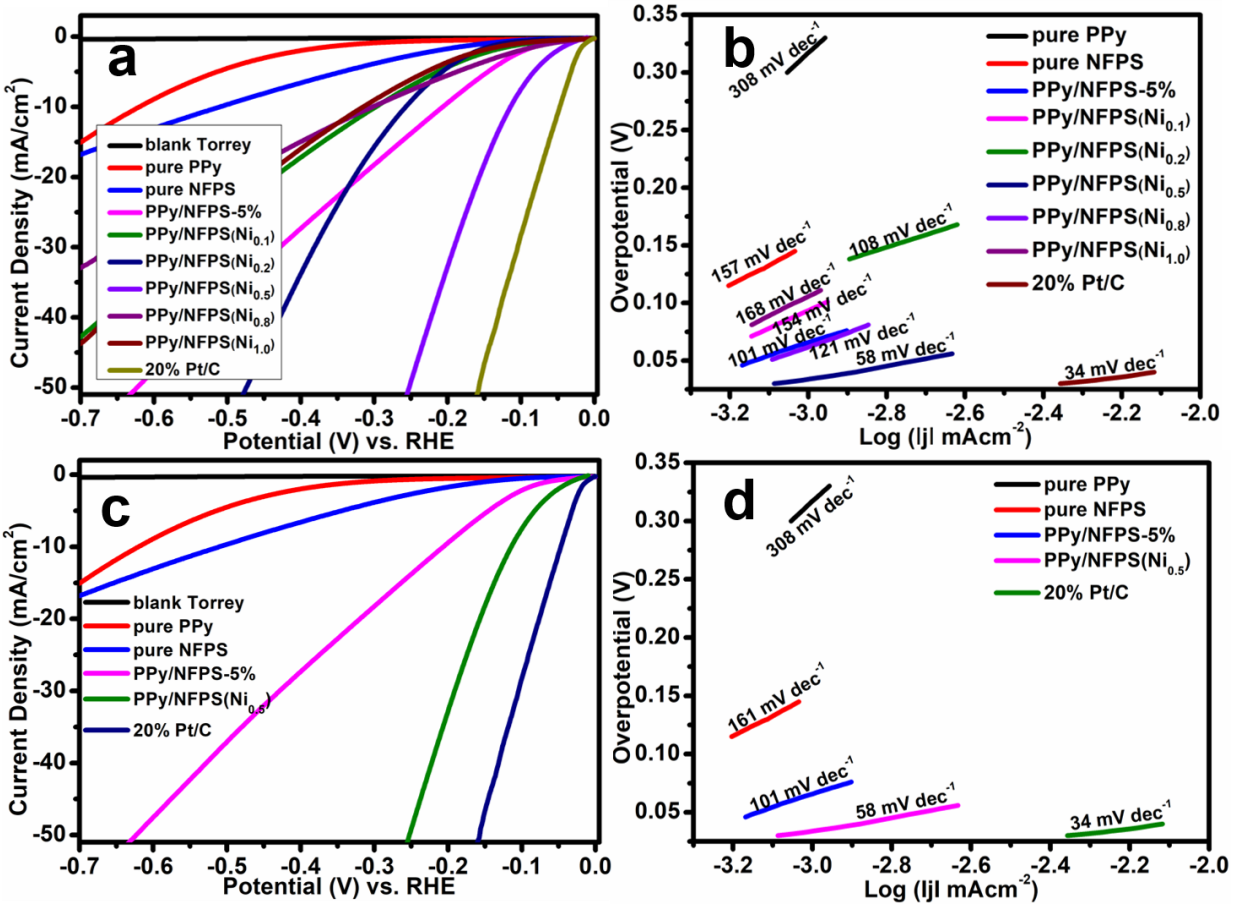

Figure 5.6: Polarization curves of (a) different PPy/NFPS(Ni_x) composites ratios, (c) PPy/NFPS-5% and PPy/NFPS($Ni_{0.5}$) along with 20% Pt/C, pristine PPy, pristine NFPS along with blank Torrey recorded at 10 mV/s in 0.5 M H_2SO_4. The Tafel slope of (b) different PPy/NFPS(Ni_x) composites ratios, (d) PPy/NFPS-5% and PPy/NFPS($Ni_{0.5}$) along with 20% Pt/C, pristine PPy and pristine NFPS.

The electrocatalytic activity of PPy/NFPS($Ni_{0.5}$) towards HER is also investigated using LSV at different scan rates for optimization (figure 5.7(a)). It has been found that PPy/NFPS($Ni_{0.5}$) shows better HER activity at a sweep rate of 10 mV/s, although onset overpotential is almost similar at different scan rates. The difference in the polarization curve with varying scan rates may be attributed to the diffusion-controlled process. [187], [192] After the electrochemical characterization, the CV cycle was repeated up to 2000 times to examine the catalytic stability

of PPy/NFPS($Ni_{0.5}$). It has been revealed that the PPy/NFPS($Ni_{0.5}$) exhibits remarkable catalytic stability toward HER after the 2000 cycle (figure 5.7(b)). The catalytic material PPy/NFPS($Ni_{0.5}$), having improved catalytic activity for HER in an acidic medium, is also studied in various electrolytic media, i.e., 0.5 M KOH (basic medium) and 0.5 M Na_2SO_4 (neutral medium) (figure 5.7(c)). It has been revealed that PPy/NFPS($Ni_{0.5}$) exhibits improved catalytic activity for HER in an acidic media, which follows the semicircle of H_2 generation. The as-synthesized PPy/NFPS($Ni_{0.5}$) is investigated for environmental stability after one year with the help of the LSV technique (figure 5.7(d)). It has been found that the catalyst is relatively environmentally stable after such a long period and has almost identical catalytic activity. The long-term catalytic stability of PPy/NFPS($Ni_{0.5}$) materials is also investigated with the help of chronoamperometry at the constant overpotential of 111 mV vs. RHE for 50000 seconds (figure 5.7(f)). It has been found that the as-synthesized PPy/NFPS($Ni_{0.5}$) offers remarkable catalytic stability and outstanding durability toward HER.

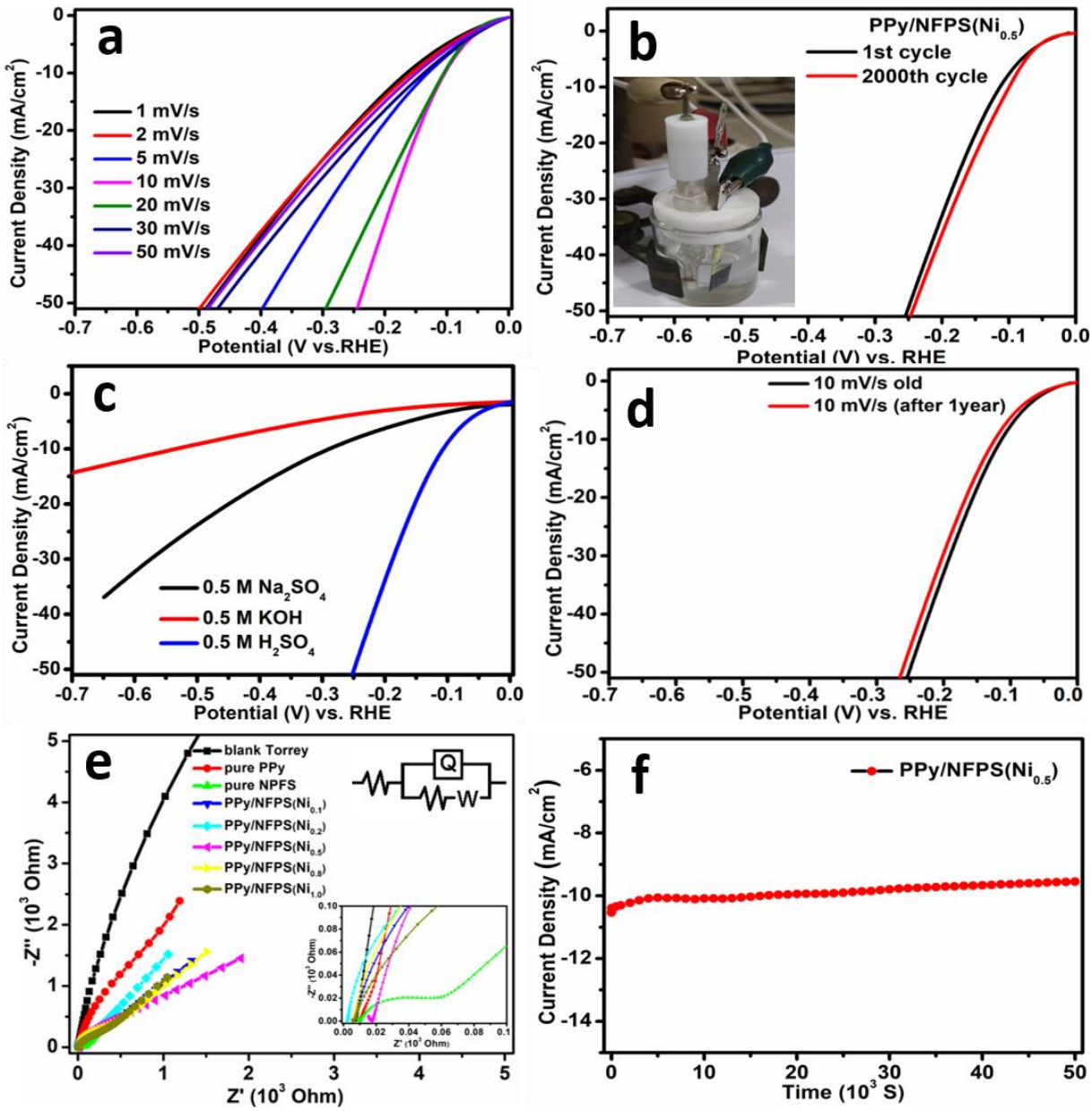

Figure 5.7: (a) LSV curve of PPy/NFPS($Ni_{0.5}$) at the different scan rate, (b) stability of LSV curve of PPy/NFPS($Ni_{0.5}$) (inset of figure7(b) shows the electrochemical setup), (c) LSV curve of PPy/NFPS($Ni_{0.5}$) in different electrolytic media, (d) environmental stability test using LSV of PPy/NFPS($Ni_{0.5}$), (e) EIS spectra of different ratios of PPy/NFPS(Ni_x) composites, inset of figure 7(e) shows the zoom view and equivalent circuit, and (f) chronoamperometry of PPy/NFPS($Ni_{0.5}$). The electrolyte used in figure 5.7 (a), (b), (d), (e) and (f) is 0.5 M H_2SO_4 solution.

The EIS method is a helpful tool for analyzing the charge transfer behavior of catalytic material. The Nyquist plots of various electrode material compositions are depicted in figure 5.7(e) using the three-electrode system in 0.5M H_2SO_4 as an electrolyte where the electrode is modified conducting carbon paper, Ag/AgCl and Pt were utilized as the reference and counter, respectively. The EIS measurement was carried out for each electrode material at their respective onset potential between 10^5 Hz and 0.01 Hz. A semicircle is observed in the high-frequency area, and a linear curve in the low-frequency for each electrode is shown in figure 5.7(e). R_{ct} (Charge transfer resistance) between the electrolyte and electrode is correlated with the diameter of the semicircle. The meeting point of the semicircle obtains Rs (Solution resistance) with a real axis in the high-frequency region.[180], [189] The ZSimpWin 3.21 software was used to evaluate and fit the impedance data for various electrodes with the help of the circuit displayed in the inset of figure 5.7(e). The solution resistance (R_s) is ca. 5-20 **Ω**. The charge transfer resistance (R_{ct}) of different electrode materials for pristine PPy, pristine NFPS, PPy/NFPS($Ni_{0.1}$), PPy/NFPS($Ni_{0.2}$), PPy/NFPS($Ni_{0.5}$), PPy/NFPS($Ni_{0.8}$), and PPy/NFPS($Ni_{1.0}$) are 3887.0 **Ω**, 33.53 **Ω**, 374.2 **Ω**, 237.5 **Ω**, 39.7 **Ω**, 364.5 **Ω**, and 264.7 **Ω**, respectively. PPy/NFPS($Ni_{0.5}$) electrode materials exhibit lower charge transfer resistance and facilitate charge intercalation and de-intercalation more easily. The migration of ions from the electrolyte into the electrode materials might be prevented due to the denser and more compact structure, which is least in the case of PPy/NFPS($Ni_{0.5}$).

ECSA (The electrochemical active surface area) of the composite PPy/NFPS($Ni_{0.5}$) for HER was investigated by computing their C_{dl} values using CV curves to examine better the electrocatalytic activity of the materials (figure 5.8). The CV (vs. Ag/AgCl) curve was taken in a non-faradic region to calculate the capacitive current using double-layer charging-discharging of samples. Figure 5.8(a, c, and e) shows the CV curve at different scan rates starting from 5

mV/s to 80 mV/s for pristine PPy, pristine NFPS, and PPy/NFPS($Ni_{0.5}$), respectively, and their current density vs. scan rate curves are shown in figure 5.8(b, d, and f) respectively. The C_{dl} values [205], [206] are calculated by plotting the anodic and cathodic current density curve vs. scan rate, as depicted in figure 5.8(b, d, and f). The anodic and cathodic slope values are calculated and then averaged to get the C_{dl} value. Therefore, the C_{dl} value of pure PPy is 6.39 mF cm^{-2} (average of both cathodic and anodic slope) figure 5.8(b), pure NFPS is 13.13 mF cm^{-2} (average of both cathodic and anodic slope) figure 5.8(d), and that of PPy/NFPS($Ni_{0.5}$) is 36.19 mF cm^{-2} (average of both cathodic and anodic slope) figure 5.8(f). It has been observed that the C_{dl} value of composite PPy/NFPS($Ni_{0.5}$) is six-fold higher than the pure PPy. The higher the C_{dl} value, the more ECSA values.[164], [205], [206], [207], [208] The improved electrocatalytic catalytic activity of PPy/NFPS($Ni_{0.5}$) is co-related to increased C_{dl} and hence ECSA value. Due to the high value of Cdl of PPy/NFPS($Ni_{0.5}$), as compared to the pristine PPy and pure NFPS, PPy/NFPS($Ni_{0.5}$) displays better catalytic activity towards HER.

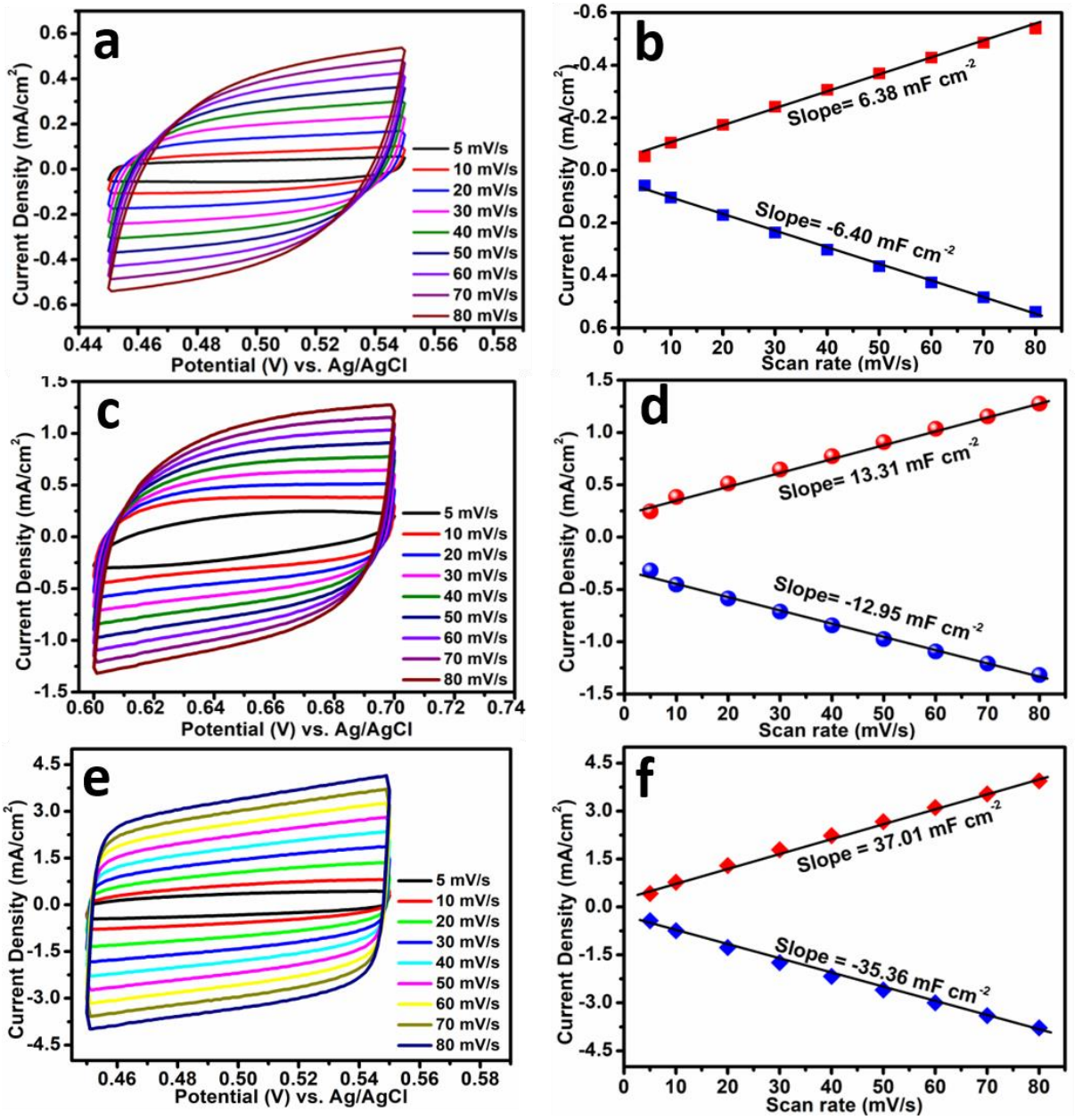

Figure 5.8: (a) CV curve of pure PPy at the different scan rate, (b) its corresponding current density vs. scan rate curve, (c) CV curve of pure NFPS at the different scan rate, (d) its corresponding current density vs. scan rate curve, (e) CV curve of PPy/NFPS($Ni_{0.5}$) at different scan rate and (f) its corresponding current density vs. scan rate curve for the estimation of electrochemical surface area (ECSA).

5.4 Conclusions:

In summary, a new composition of materials (PPy/NFPS(Ni_x)) was synthesized by conventional oxidative *in-situ* polymerization technique from polypyrrole and Ni-doped NASICON structure NFPS($Ni_{0.5}$), $Na_3Ni_{0.5}Fe_{1.5}(SO_4)_2(PO_4)$. XRD investigation assured rhombohedral phase of NFPS($Ni_{0.5}$) retained in PPy/NFPS($Ni_{0.5}$) composites. NFPS(Ni_x) incorporation into the PPy matrix is confirmed via SEM images and elemental analysis (EDAX and mapping). The enhanced electrical conductivity arises from the synergistic effect between NFPS(Ni_x) and PPy. Incorporating NFPS(Ni_x) into the PPy matrix contributes to the improvement in electrocatalytic performance for HER. The PPy/NFPS($Ni_{0.5}$) (optimized ratio for Ni) shows a much better electrocatalytic activity towards HER than other ratios. The onset overpotential for PPy/NFPS($Ni_{0.5}$) is -13 mV vs. RHE and a lower Tafel slope value of 58 mV dec^{-1} (considerably smaller than pure PPy and pure NFPS), which is comparable to Pt/C and better than most of the recently published polymer-based HER catalyst. Also, it exhibits a current density of 10 mA/cm^2 at a markedly lower overpotential of -111 mV, which is quite good than other composite ratios. The PPy/NFPS($Ni_{0.5}$) nanocomposite offers long-sustaining environmental and catalytic stability and impressive durability. According to the electrochemical findings, composites made of PPy/NFPS($Ni_{0.5}$) are a strong contender for electrocatalytic HER in the real world.